Electronic Supplementary Material (ESI) for Soft Matter.

Transient shape morphing of active gel plates: Geometry and physics
Supplementary Material

Valentina Damioli[1], Erik Zorzin[1], Antonio DeSimone[1,2,3], Giovanni Noselli[1], and Alessandro Lucantonio[2,3]

[1]SISSA–International School for Advanced Studies, 34136 Trieste, Italy.
[2]The BioRobotics Institute - Scuola Superiore Sant'Anna, 56127 Pisa, Italy.
[3]Department of Excellence in Robotics & AI, Scuola Superiore Sant'Anna, 56127 Pisa, Italy.

Contents

1 Captions of Supplementary Videos

SV 1: Transient shape evolution of gel samples of type I, II, and III during swelling experiments. The time-lapse consists of snapshots from the lateral camera taken at a frame rate of 1 frame/s.

SV 2: Transient shape evolution of gel samples of type I, II, and III during shrinking experiments. The time-lapse consists of snapshots from the lateral camera taken at a frame rate of 1 frame/s.

2 Digital photomasks for the fabrication of homogeneous and heterogeneous samples

We report below two figures showing the digital photomasks that were employed for the fabrication of the homogeneous (Fig. S1) and of the heterogeneous gel samples (Fig. S2).

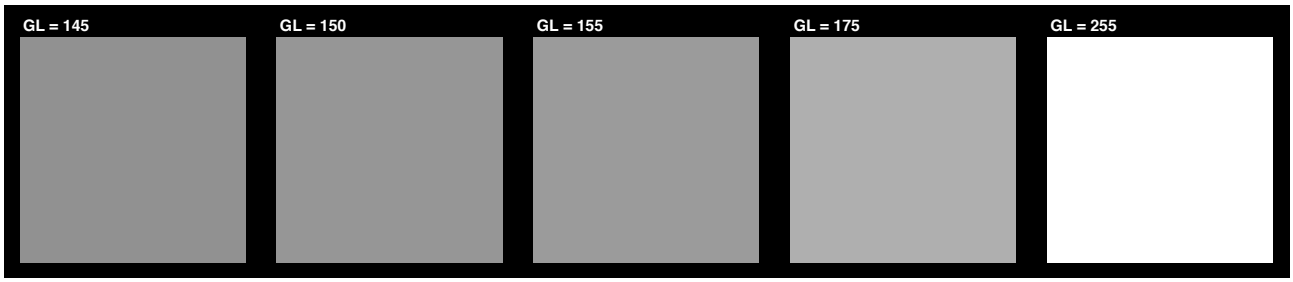

Fig. S1: Digital photomasks employed for the fabrication of the homogeneous gel samples with GL $= \{145, 150, 155, 175, 255\}$.

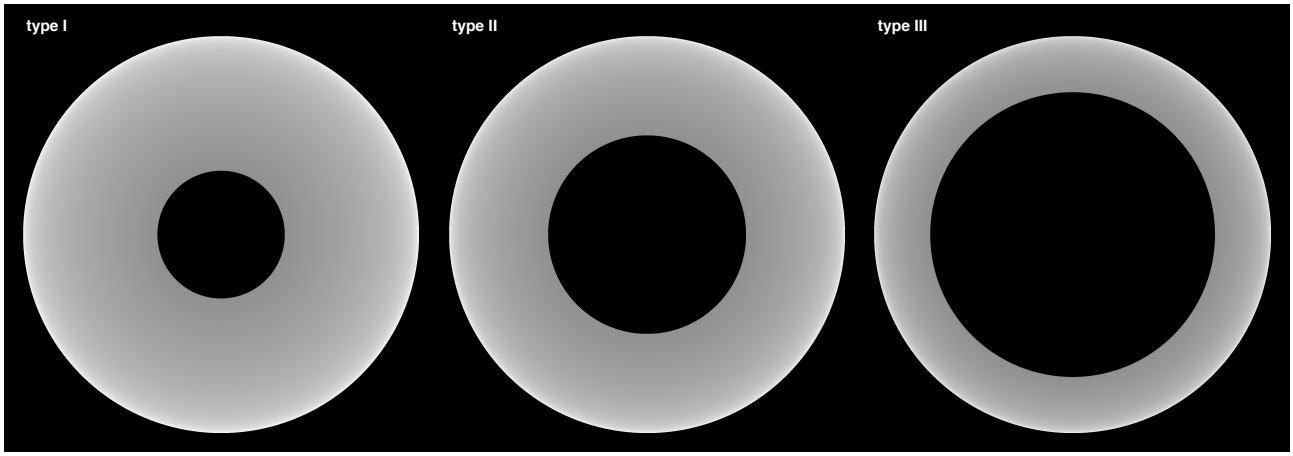

Fig. S2: Digital photomasks employed for the fabrication of the heterogeneous gel samples of type I, II, and III.

3 Measurement of the azimuthal stretches as a function of time

Snapshots from the top camera allowed to compute the azimuthal stretches at the rims of the heterogeneous gel samples during the transient shaping, using a semi-automatic, post-processing algorithm developed in ImageJ (version 1.53g, Wayne Rasband and contributors, NIH, USA). As detailed in the following, the algorithm is based on the determination of the radial coordinates ρ_i and ρ_o that correspond to the inner and outer rims, respectively, of the mid surface of a gel plate. As shown by Eq. $(5)_2$ of the main text, such radial coordinates are directly related to the corresponding azimuthal stretches ρ_i/r_i and ρ_o/r_o, where r_i and r_o are the initial radii.

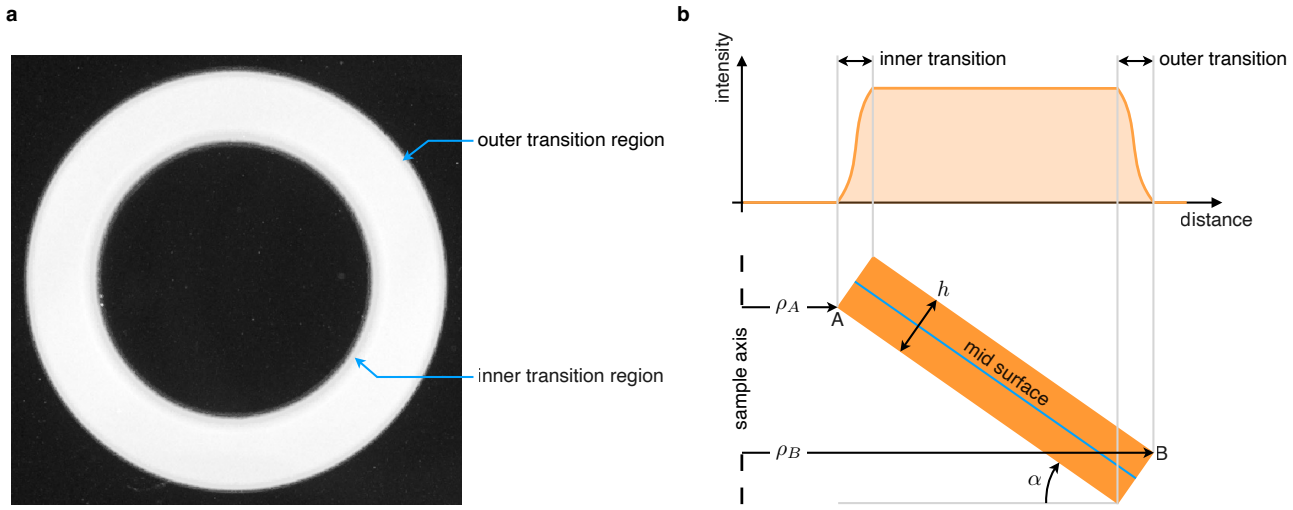

Fig. S3: (a) Typical top view of a gel sample with indication of the inner and outer transition regions in the image and (b) a graphical description of the effect of the gel samples edges on the image intensity profile.

Regarding the images from the top camera, these consist of a bright annulus on a dark background and two transition regions at the sample edges where the pixel intensity smoothly varies between two tones (Fig. S3a). These transition regions are due to the fact that the gel samples are semi-transparent, and they correspond to the project of the thickness of the plate on the image plane (Fig. S3b). Hence, the radial coordinate of the mid surface may be computed as the distance of the center of the corresponding transition zone.

In the image post-processing script, the transition zones are identified and their centers computed through the analysis of the radial intensity profile in the images. Specifically, the algorithm consist in the following steps:

1. gray-scale images are converted into binary images (with zero intensity level for the background and maximum

intensity level for the sample) to remove spatial noise and to determine the centroid of the sample image;

2. on the original gray-scale images, radial intensity profiles are computed along a family of 100 segments equally spaced in the angular direction and departing from the sample centroid;

3. the average intensity profile is computed and then clipped by user-defined low and high thresholds chosen to suitably isolate the two transition zones;

4. the radial coordinates at which the intensity crosses the thresholds are recorded to define the boundaries of each transition zone;

5. finally, the radial coordinates (ρ_i, ρ_o) corresponding to the centers of the transition zones are computed as the averages of the coordinates of the boundaries.

This algorithm was exploited for the semi-automatic analysis of all the image stacks corresponding to the samples of type I and II to eventually determine the time-courses of the stretches at their inner and outer rims (see Fig. 9a,b of the main text). Clearly, application of the algorithm was limited to the analysis of axisymmetric configurations. For samples of type III, namely those achieving a cylindrical configuration at equilibrium, application of the algorithm was hindered by the occurrence of partial overlapping between the transition regions at large times, when the base angle attained a critical value. Hence, for samples of type III, the determination of the stretches required the use of an alternative approach at large times. In particular, information regarding the base angle α (from the lateral camera) and the thickness h was exploited in combination with the knowledge of the radial distances ρ_A and ρ_B of the points A and B (see Fig. S3b) to compute the stretches at the rims as $(\rho_A + h/2\,\sin\alpha)/r_i$ and $(\rho_B - h/2\,\sin\alpha)/r_o$.